Supplementary information

Flame doping of indium ions into TiO_2 nanorod array for enhanced solar water oxidation

Xue Chen[a], Biyi Chen[a], Dan Li[a], Longhua Li[a], Dongbo Xu [a]* and Weidong Shi[a]*

a School of Chemistry and Chemical Engineering, Jiangsu University, Zhenjiang city 212013, P. R. China

*Corresponding author, *E-mail addresses*: xudb39@ujs.edu.cn, swd1978@ujs.edu.cn

EXPERIMENTAL SECTION

Preparation of TiO_2 and Flame doping In- TiO_2.

The precursors were homogeneously dispersed on FTO glass using the spin coating strategy and the used experimental parameters of 3000 rpm and 25 s were used. After that precursor coated FTO glass was dried in a 100 °C oven to eliminate glycol, the above operations were operated repeatedly 10 times. Lastly, the precursor-coated FTO glass (and 1 × 1 cm^2 in area with 1.5 mm thickness) was annealed in a flame and the used FTO was set at 5 cm above the micro-combustor (CAMPSOR-918) for 20 s. The butane and air were used to burn to provide flame, as well as the mass flows, were set at 30 and 135 g h^{-1}, respectively.

Material characterization.

The crystallinity was detected by using a D8 ADVANCE X-ray Diffraction (XRD, Bruker D8 Advance, 10–80°, 5° min^{-1}) instrument. The UV-vis diffuse reflectance spectra were collected on UV2450 UV spectrophotometer. The surface morphology was observed by a JSM-7001F field emission scanning electron microscopy (FESEM). The microstructure was characterized by a Tecnai G2 F30 high-resolution transmission electron microscopy (HRTEM). The surface electronic structure was determined by an ESCALAB 250 Xi X-ray photoelectron spectroscopy (XPS), with standard C 1s peaks (284.8 eV) to calibrate. The surface impurities were investigated by a DRX Lase Raman spectrometer. Steady-state/time-resolved fluorescence was performed using an Edinburgh FLS 1000 fluorescence spectrometer with an excitation wavelength of 380 nm and an emission wavelength. The EDX images were recorded using a Thermo

Fisher Scientific field emission electron microscope equipped with an energy spectrometer -QUANTAX 200, with a voltage of 10 kV and a current of 1 nA. ARXPS measurements (Thermo Scientific K-Alpha) were performed in an ultrahigh vacuum (~10^{-9} Torr) with varying TOA from 5° to 60°.

PEC measurement.

The PEC measurements were measured with a CHI 760e electrochemical workstation and the illumination was supported by a xenon lamp (The CEL-HXF30 xenon lamp light source of China Education Jinyuan Company has an electric power of 300 W, and the actual irradiation to the surface power of the photoelectric aurora is 100 mW/cm^2.), in which the resultant photoelectrodes, an Ag/AgCl electrode and platinum wire were utilized as the working electrodes, reference electrode and counter electrode, respectively. The light power beaming on the photoanode was tuned to 100 mW cm^{-2} and 0.5 M Na_2SO_4 (pH = 6.8) was used as an electrolyte for all PEC measurements. The light intensity was measured using a calibrated photodetector (CEAULIGHT CEL-NP2000). The photodetector was placed at a fixed distance from the light source, and the measured light intensity was then used for our photoelectrochemical experiments. The applied bias was converted to a reversible hydrogen electrode (RHE) according to the equation (1):

$$E_{RHE} = E_{Ag/AgCl} + 0.059\ pH + 0.197 \quad (1)$$

where E_{RHE}, $E_{Ag/AgCl}$ are the RHE (V) and the applied potential (V), as well as the pH of the electrolyte. The scanning rate of 50 mV s^{-1} was chosen to evaluate the linear sweep voltammetry (LSV) curves. The electrochemical impedance spectroscopy (EIS)

was performed at the frequency ranges from 10^5 to 10^{-2} Hz under light irradiation. The Mott-Schottky analysis was performed in the dark and the frequency of 10^3 Hz and rate of 10 mV s^{-1} were used, respectively. The conversion efficiency of incident photons to current (IPCE) is recorded in the Quantum Efficiency Evaluation system (Newport/Oriel, QE-PV-SI). IPCE spectra were measured at a constant potential (1.23 V vs. RHE) in the wavelength range of 300 ~ 600 nm and the values are calculated was calculated using the following equation (2):

$$\text{IPCE}\ (\%) = 1240j/P_{light}\lambda \quad (2)$$

, where the j (mA cm^{-2}) was the measured current density, the P_{light} was the given radiation power of 100 mW cm^{-2}, λ was the wavelength of monochromatic light. Surface charge separation efficiencies ($\eta_{surface}$) was deducted using equation (3):

$$\eta_{surface}\ (\%) = j(Na_2SO_4)/j(Na_2SO_3) * 100\% \quad (3)$$

, where the $j(Na_2SO_4)$ and $j(Na_2SO_3)$ are the measured current density in the 0.5 M Na_2SO_4 electrolyte with and without 0.5 M Na_2SO_3. The ABPE value was obtained by using the equation (4):

$$\text{ABPE}\ (\%) = (1.23\ \text{V} - E_{RHE}) * j \quad (4)$$

, where the meanings of j and E_{RHE} are the same above. Under Xe light illumination, the electrochemical impedance spectroscopy (EIS) sampling rate would range from 0.01 Hz to 1000 kHz. The Nyquist plot measurements were conducted at a fixed potential, which was provided by an open-circuit voltage test. Mott-Schottky studies were conducted with a frequency of 1 kHz and a scan rate of 10 mV s^{-1}. The Mott-Schottky analysis was performed under dark conditions using an AC amplitude of

0.005V. The surface charge density was calculated following equation (5):

$$N_{\mathrm{d}} = \frac{2}{e\varepsilon_0\varepsilon_r} \times \frac{dE}{d(1/C^2)} \tag{5}$$

where the N_{d} is the carrier density and can be acquired from the curves of the $1/C^2$ *vs*. *E*, *e* is the elementary charge (1.603×10^{-19} C), ε_0 is 114 for TiO_2, the ε_{r} is permittivity in a vacuum and valued of 8.854×10^{-12} F m^{-1}, E_{RHE} is the RHE and *C* is the interface capacitance formed by semiconductor and electrolytes.

Temperature simulation

The ANSYS ICEM software was employed to plot the grid and the simulation calculations were conducted in ANSYS FLUENT software. All calculations and simulations were performed under an assumed steady-state model. The discretized control equations used herein were SIMPLE method and the pressure-velocity couple was solved by the Phase Coupled SIMPLE method. The FTO upper surface and the bottom surface were set at the convective boundary and adiabatic interface to the surrounding wall, respectively.

DFT calculations

The DFT calculations were conducted in the Vienna Ab initio Simulation Package (VASP)[1]. The Perdew-Burke-Ernzerhof (PBE) exchange correlation function within a generalized gradient approximation (GGA) was used and the cutoff of 520 eV was set. The pseudopotential of projector augmented plane wave (PAW) method was used to interchange ion electron interactions[2]. The convergence threshold was set to 10^{-5} eV

and 0.02 eV $Å^{-3}$ in geometric relaxation and energy, respectively. A 3*3*2 supercell of rutile TiO_2 including 108 atoms was constructed and a vacuum length of 20 Å along z-direction was employed to eliminate interactions between mirror images[3]. The Brillouin zone was sampled by a Gamma *k*-point mesh of 1*1*1 and 3*3*1 for geometry optimizations and energy, respectively[4]. The adsorption energy (*E*ad) over H_2O molecules was calculated by the following equation (6):

$$E(\text{ad}) = E(\text{slab}*H_2O) - E(\text{slab}) - E(H_2O) \quad (6)$$

, where the $E(\text{slab}*H_2O)$, $E(\text{slab})$ and $E(H_2O)$ represent the calculated energy of the slab absorbed H_2O molecule, slab and free water molecules, respectively.

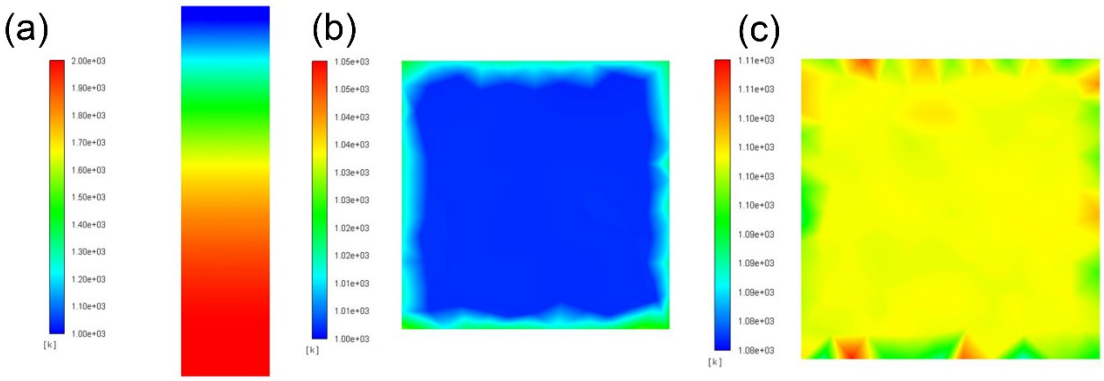

Fig S1. (a) The flame temperature along with axial spatial distribution, the height is 5 cm. The simulated temperature of the bottom (b) and upper (c)surface of FTO substrate.

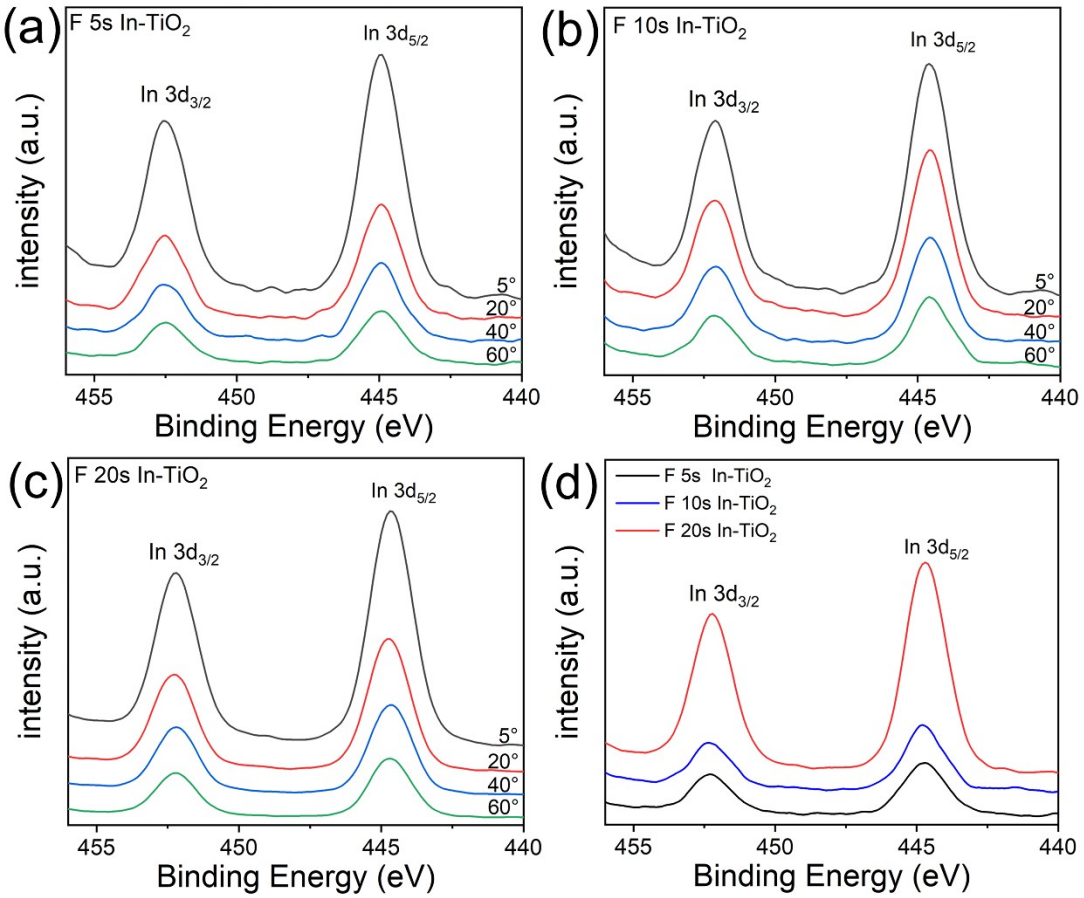

Fig S2. Angle-resolved X-ray photoemission spectroscopy of (a) F 5s In-TiO_2, (b) F 10s In-TiO_2, (c) F 20s In-TiO_2. (d) samples with different doping time lengths at a take-off Angle of 60°.

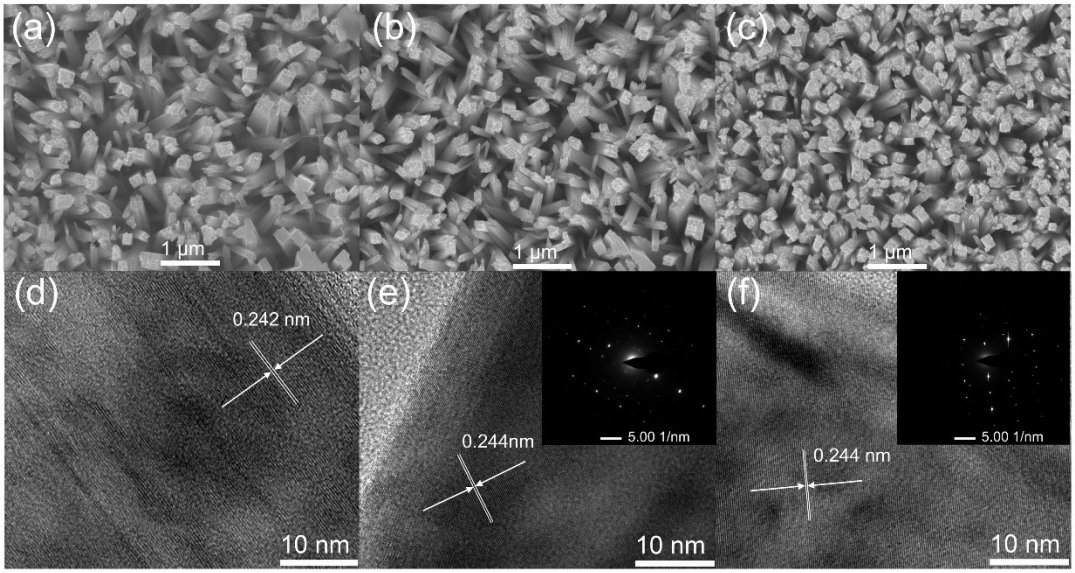

Fig S3. FESEM and corresponding HRTEM images of (a) (d) TiO_2, (b) (e) BE-TiO_2 and (c) (f) In-TiO_2. The insets are corresponding select electron diffraction patterns.

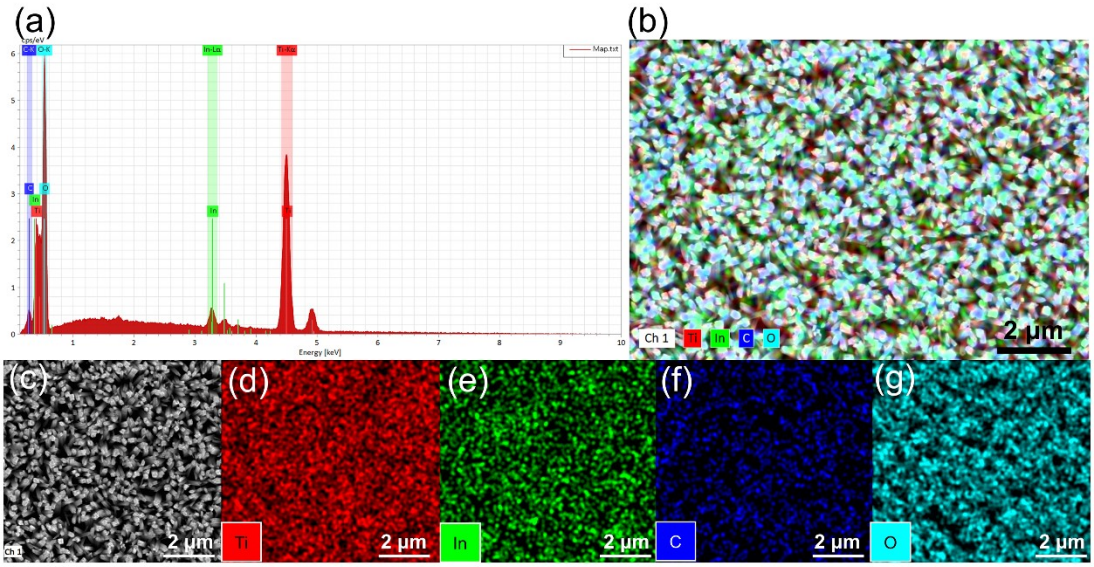

Fig S4. (a) Energy-dispersive X-ray spectrum diagram, (b) the overall spectrum diagram of the element mapping, (c) SEM image of In-TiO_2 without element mapping, the element maps of (d) Ti, (e) In, (f) C, and (g) O.

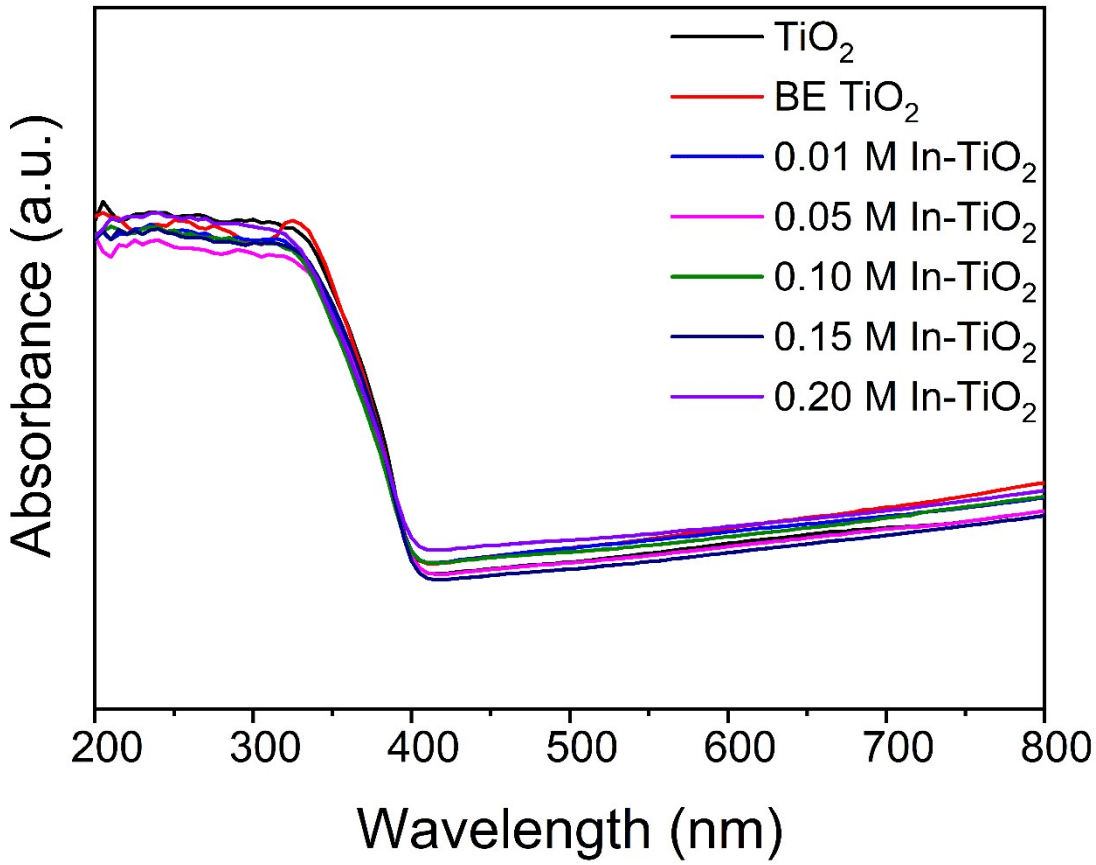

Fig S5. The UV-vis diffuse reflectance spectra of the pristine TiO_2, BE TiO_2, the In-TiO_2 with gradient concentration.

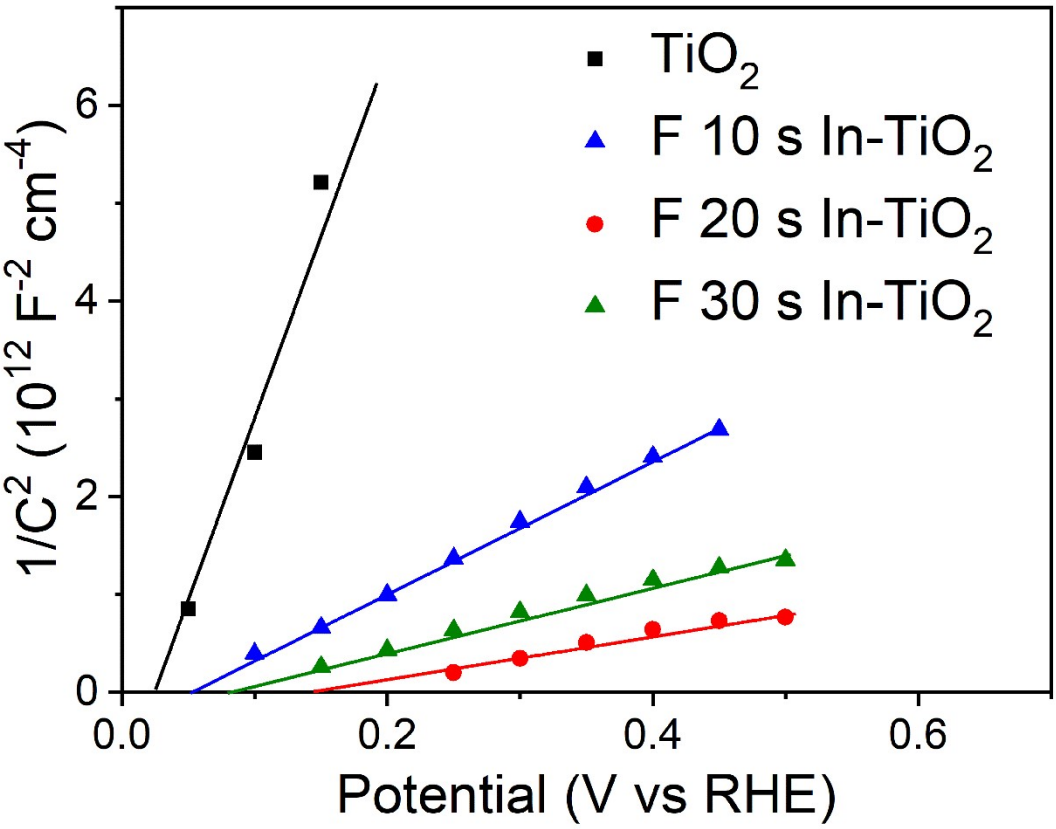

Fig S6. Mott-schottky diagram of TiO_2 and In- TiO_2 with flame doping duration of 10s, 20s, 30s.

Table S1. The atomic content of Ti, In, C, O in samples with different flame doping times.

	Ti (%)	In (%)	C (%)	O (%)
5s	32.36	0.46	2.1	65.08
15s	30.4	0.89	2.11	66.6
20s	31.17	1.11	2.17	65.55
25s	30.7	0.69	4.74	63.87
30s	29.87	0.68	4.79	64.66

Table S2. The fitted values of using the Randall circuit diagram of the TiO_2 photoanode.

	R_s/Ω	R_{ct}/Ω
pristine TiO_2	17	8916
In-TiO_2	15	1133

Reference

1 G. J. C. M. S. Henkelman, 2006, **36**, 354-360.

2 B. Hammer, L. B. Hansen and J. K. J. P. r. B. NÃ¸rskov, 1999, **59**, 7413.

3 S. J. J. o. c. c. Grimme, 2006, **27**, 1787-1799.

4 J. r. J. J. o. c. c. Hafner, 2008, **29**, 2044-2078.